Volume 23, No 2 | International Journal of Radiation Research, April 2025

Evaluation of PD-L1 expression status in nasopharyngeal carcinoma by 18F-FDG PET/CT radiomics analysis

S. Yang[1*], L. Li[2], H. Li[3], Y. Li[1]

[1]*Department of Nuclear Medicine, the First Affiliated Hospital of Guangzhou University of Chinese Medicine, Guangzhou, Guangdong 510405, China*
[2]*Department of Nuclear Medicine, the Third People's Hospital of Mianyang City, Sichuan Mental Health Center, Mianyang, Sichuan 621000, China*
[3]*PET Center, Nanfang Hospital, Southern Medical University, Guangzhou, Guangdong 510515, China*

► ***Original article***

***Corresponding author:**
Shaoxi Yang, M.M.,
***E-mail:** nfyyysx@126.com*

Received: September 2023
Final revised: February 2024
Accepted: April 2024

Int. J. Radiat. Res., April 2025; 23(2): 447-454

DOI: 10.61186/ijrr.23.2.26

Keywords: *Nasopharyngeal Neoplasms, Immune Checkpoint Inhibitors, Radiomics, Positron Emission Tomography Computed Tomography.*

ABSTRACT

Background: We aimed to accurately and efficiently evaluate Programmed Death Ligand-1 (PD-L1) expression by relevant radiomic studies of fluoro-18-fluorodeoxyglucose (18F-FDG) Positron Emission Tomography/Computed Tomography (PET/CT) images in nasopharyngeal carcinoma (NPC) patients. ***Materials and Methods:*** This retrospective study included 60 untreated NPC patients had PET/CT. Cohorts of training and validation were randomly selected among the patients. The CT and PET radiomic features from the training cohort were obtained and screened, to construct CT, PET and combined models. Finally, verification and comparative analysis were performed. ***Results:*** According to the analysis, the maximum Standardized Uptake Value (SUVmax) alone was the standalone predictive indicator of PD-L1 presence level, thus incorporated into the combined model. Among our training cohort, the CT, PET, and combined models' Area under Curve (AUC) values respectively were 0.837, 0.852, and 0.948, demonstrating excellent discrimination and calibration. However, the combined model had higher AUC values in the cohorts of training and validation, reaching AUCs of 0.948 and 0.802, respectively. Clinical decision curve analysis (DCA) further illustrated Combined model surpassed both the CT and PET models, attaining a benefit threshold probability of more than 5% and a net benefit (NB) of 0.450 at the optimal threshold probability. ***Conclusion:*** The combined predictive model based on relevant radiomic studies of PET/CT scans performed better than other models in assessing individualized PD-L1 expression in NPC.

INTRODUCTION

NPC is an aggressive carcinoma that arises from the nasopharynx's columnar epithelium mucosa. The illness has a noticeable geographic dispersion and is linked to both environmental and genetic factors. It is most common in northern Africa, southern China, and southeast Asia. Even while NPC incidence has decreased recently worldwide, in endemic areas it remains one of the primary reasons of malignancy and cancer-related mortality [1-3]. Among these high-prevalence areas, the most common histopathological subtype of nasopharyngeal carcinoma is nonkeratinizing squamous cell carcinoma, relating with the Epstein-Barr Virus (EBV) [1, 4]. Historically, locally and early advanced NPC were primarily treated with radiotherapy alone or in combination with chemotherapy. Patients are prone to distant metastasis or local recurrence and exhibit a poor response to conventional treatment and poor prognosis due to chemotherapy resistance [1, 5-8]. However, with the rapid development and breakthrough of immune checkpoint blockade therapy for solid neoplasm, immunotherapy targeting PD-L1/PD-1 (Programmed Death-1) has become a recent research hotspot. Several clinical trials and research have shown that PD-L1/PD-1 inhibitor single therapy as also as combination with chemotherapy or radiotherapy have improved efficacy and prognosis in the antitumour treatment of NPC [9-15]. In 2021, China approved PD-L1/PD-1 inhibitors in the metastatic, recurring, or resistant nasopharyngeal cancer as a first-line recommendation. These inhibitors, combined with cisplatin and gemcitabine, are now recognized as one of the new standard first-line recommendations, providing advanced NPC patients with new hope for successful treatment [16].

Before undergoing immunotherapy, PD-L1 expression is evaluated via immunohistochemistry (IHC) on tumor tissue samples, which can be invasive and affected by tumor heterogeneity [17]. Therefore, developing a noninvasive and accurate method for assessing PD-L1 expression status is particularly important for predicting and screening tumor patients who may gain from immunotherapy. As a

[Downloaded from ijrr.com on 2026-10-30]

[DOI: 10.61186/ijrr.23.2.26]

rapidly developing emerging field, radiomics has achieved remarkable results in genophenotype prediction, prognosis monitoring, treatment plan decision-making, tumor staging and grading, disease diagnosis and differential diagnosis, and efficacy evaluation [18-21]. Several studies have utilized radiomic features, including MRI (Magnetic Resonance Imaging), CT, and PET/CT to develop prediction models for PD-L1 expression with several cancer forms, like non-small cell lung carcinoma (NSCLC) [22-27], breast carcinoma [28], early-stage lung adenocarcinoma [29], hepatocellular carcinoma [30], gastric adenocarcinoma [31, 32], and renal clear cell carcinoma [33]. However, to our knowledge, no studies have developed radiomic-related predictive models for PD-L1 expression in NPC.

Therefore, our goal in this research was to construct an effective personal prediction model for nasopharyngeal cancer patients' PD-L1 expression by analyzing the radiomic characteristics of PET/CT, and the important relevant metabolic and clinicopathological characteristics to screen patients who may profit from immunotherapy. This study's novelty lies in being the first attempt to noninvasively forecast the PD-L1 expression in NPC through combining radiomics and PET/CT.

MATERIALS AND METHODS

Patients

We retrospectively analyzed 60 individuals had ^{18}F-FDG PET/CT scans at the First Affiliated Hospital of Guangzhou University of Chinese Medicine from June 2021 to April 2023 and were pathologically confirmed to have NPC. The following were the inclusion criteria: (1) pathologically confirmed nasopharyngeal carcinoma and PD-L1 IHC examination; (2) Examination with PET/CT within 2 weeks before the biopsy and treatment; and (3) full clinical and other pathological information, such as gender, age, smoking history, plasma EBV-DNA quantification before treatment, Ki-67 expression, EBER and tumor stage. The following were the exclusion criteria: (1) received any antitumour therapy, such as radiotherapy or chemotherapy, prior to ^{18}F-FDG PET/CT and/or pathological examination; (2) possessed a prior medical history of cancerous tumors; and (3) had incomplete clinical and pathological data. The eighth eversion of staging system developed by AJCC (American Joint Committee on Cancer) was used, and PET/CT scans and related clinicopathological information were collected from all patients. Computer-generated random numbers were employed to separate individuals into the cohorts for validation and training at a 1:2 ratio.

Detection of PD-L1 expression

Surgical specimens or biopsy were embedded in paraffin, formalin-fixed, and then cut at a thickness of 4 μm in serial sections. PD-L1 expression was measured using an automated immunohistochemistry stain (Roche BenchMark XT, USA) and a detection kit (SP263 pharmDx, USA) and was evaluated separately by two pathologists who did not have access to the clinical information. The calculation method utilized was the TPS, in which the overall quantity of viable tumorous cells was divided by the count of PD-L1-positive tumorous cells and then expanded by 100 fold. A result of ≥50% was defined as high expression.

PET/CT imaging

Before PET/CT, patients had to keep their fasting blood sugar levels under 11 mmol/L and to fast for at least 6 hours. Following a venous infusion of 3.70–5.55 MBq/kg ^{18}F-FDG (^{18}F-FDG I.V. Injectable Solution, Atom Hi-Tech, CN) and quiet rest for 1 hour, data acquisition was executed using a PET/CT system (GE Discovery MI, USA). A CT scan was conducted using the following parameters: 120 kV of voltage, 120 mA of current, 70 cm of warp field of view (FOV), 0.984:1 pitch, 0.8 s of rotation time, 3.75 mm of slice thickness, 512 x 512 matrix. This was followed by a PET scan, which took 7-8 beds per patient and 2-3 minutes per bed.

Image segmentation and radiomic feature extraction

LIFEx software (LIFEx 7.3.0 software, FR) was utilized for importing those DICOM-formatted PET and CT images [34]. Two highly skilled nuclear medical experts manually mapped the primary tumor to obtain a three-dimensional VOI (Volume of Interest) layer by layer and determined TLG (Total Lesion Glycolysis) and MTV (Metabolic Tumor Volume) at a threshold of forty-one percent of SUVmax. MRI and Contrast-enhanced CT are sometimes used to help determine the VOI. The spatially resampled voxel size was 1×1×1 mm^3. The CT image was discretized to 400 in the absolute range of -1000 to 1000, while the PET image was discretized to 64 in the absolute range of 0 to 30. Subsequently, radiomic feature extraction was carried out. Utilizing the intraclass correlation coefficient (ICC), the features' repeatability and dependability were assessed, and patients with an ICC>0.75 were retained. The extracted feature values were normalized using the "StandardScaler" function in the open-source software Python (Python 3.8 software, NL) "sklearn Preprocessing" module.

Radiomics feature selection and machine learning model construction

Those useful PET and CT features were selected separately from our training group using LASSO (Least Absolute Shrinkage and Selection Operator). The univariate analysis served to compare clinicopathological indicators (including gender, age,

[Downloaded from ijrr.com on 2026-10-30]

[DOI: 10.61186/ijrr.23.2.26]

smoking history, pretreatment plasma EBV-DNA concentration, Ki-67 expression, the EBER, and tumour stage) and related metabolic parameters (including the MTV, TLG, and SUVmax) between the groups with low and high PD-L1 presence among our training cohort, and the multivariate logistic analysis subsequently served to determine the standalone predictive indicator substantially linked with PD-L1 expression. The support vector machine (SVM) in the Python 3.8 "sklearn" module was used to construct CT, PET and combined machine learning models. The SVM model was established using an internal matrix laboratory (MATLAB) script, the linear kernel function was selected, the penalty coefficient C was assigned to 1, and the parameters were adjusted by two 3-fold cross-validations. Figure 1 shows the model-building process used in our study.

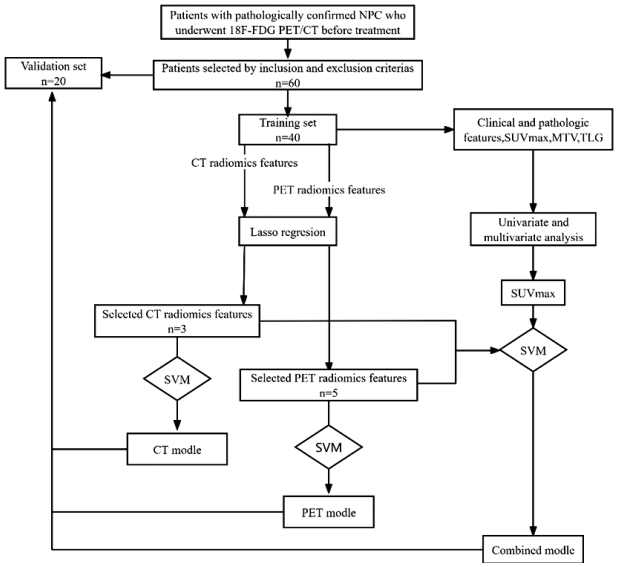


Figure 1. Study flowchart of 18F-FDG PET/CT radiomics analysis for predicting PD-L1 in nasopharyngeal carcinoma. (18F-FDG PET/CT, fluoro-18-fluorodeoxyglucose positron emission tomography/computed tomography; PD-L1, programmed death ligand-1; NPC, nasopharyngeal carcinoma; SUVmax, maximum standardized uptake value; MTV, metabolic tumor volume; TLG, total lesion glycolysis; Lasso, least absolute shrinkage and selection operator; SVM, support vector machine;).

Performance evaluation of machine learning models

Across the training and validation samples, the ROC (Receiver Operating Characteristic) curve and AUC were employed for evaluating models, and sensitivity and specificity were calculated. Hosmer-Lemeshow test was applied to evaluate the fitness of the model. AUC values comparing different models was subjected to the DeLong test. By computing NB of a number of threshold probabilities throughout the cohort, DCA was employed for evaluating a model's therapeutic value.

Statistical analysis

SPSS statistical analysis software (SPSS 23.0 software, USA) was dedicated to univariate analysis (including independent sample t test, chi-square test, or Mann–Whitney U test) and multivariate logistic analysis. A P-value of less than 0.05 in a bilateral test was the criterion for statistical significance. Open-source Python 3.8 software was employed to statistically analyze radiomic features. The "pingouin" module was used for ICC calculations, the "LassoCV" in the "sklearn.linear_model" module was used for LASSO regression analysis, and the "roc_curve" and "roc_auc_score" functions in the "sklearn.metrics" module were used for ROC curve plotting and AUC calculation, respectively. In addition, we used R statistical software (R 4.0.2 software, NZ) for the Hosmer–Lemeshow test, Delong test, and DCA curve plotting.

RESULTS

Clinicopathological features and related metabolic parameters

Among 60 NPC individuals, the average age was 51.65 years, ±11.59 years, with a male dominance of 2:1. 42 patients (70.0%) were in TNM stage III-IV, and 36 (60.0%) exhibited high levels of PD-L1. All the nasopharyngeal carcinoma lesions displayed metabolic enhancement on ^{18}F-FDG PET/CT, with a SUVmax of 11.13±6.25. Figure 2 displays a PET/CT image from one such patient. In table 1, all patients' clinicopathologic and associated metabolic indicators are summarized, and univariate examination failed to uncover any substantial disparities (P>0.05) in these aforementioned indicators between the training and validation sets, signifying a balanced distribution of baseline factors for both cohorts.

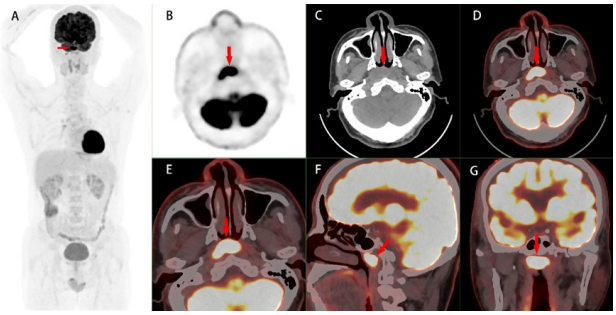


Figure 2. A 58-year-old male patient with nasopharyngeal carcinoma. The red arrow indicates a nasopharyngeal carcinoma lesion. PET showed obvious hypermetabolic foci in the nasopharynx, and SUVmax was 20.4, and CT showed obvious thickening, swelling and density reduction of the soft tissues of the nasopharynx.

In the training cohort, PD-L1 level was high in 60.0% (24 patients) and low in 40.0% (16 patients). The SUVmax values for PD-L1 high-level group and low-level group were 13.17±6.27 and 7.06±4.58, respectively. Within the training cohort, univariate analysis showed the PD-L1 level did not correlate

[Downloaded from ijrr.com on 2026-10-30]
[DOI: 10.61186/ijrr.23.2.26]

with gender, age, smoking history, EBVDNA quantification, or EBER (P>0.05; table 2); however, it was significantly associated with Ki-67 expression, TNM stage, SUVmax, MTV, or TLG (P<0.05; table 2). Further multivariate logistic analysis ultimately demonstrated the SUVmax alone was the independent predictor of PD-L1 expression status (OR (Odds Ratio)=1.295, 95% CI (Confidence Interval)=1.074-1.562, P=0.007). Therefore, only the SUVmax was used for the subsequent construction of combination prediction model.

Table 1. The clinicopathological features and related metabolic parameters of the training cohort and validation cohort. (EBV, Epstein-Barr virus; EBER, EBV-associated RNA; PD-L1, programmed death ligand-1; SUVmax, maximum standardized uptake value; MTV, metabolic tumor volume; TLG, total lesion glycolysis).

Variables	Total (n=60)	Training (n=40)	Validation (n = 20)	Statistics	P
Age (years)	51.65± 11.59	51.95± 11.73	51.05± 11.58	t=0.281	0.779
Sex				c^2=0.038	1.000
Male	40(66.7%)	27(67.5%)	13(65.0%)		
Female	20(33.3%)	13(32.5%)	7(35.0%)		
Smoking history				c^2=1.227	0.326
Smoker	13(21.7%)	7(17.5%)	6(30.0%)		
Never	47(78.3%)	33(82.5%)	14(70.0%)		
EBV-DNA				c^2=0.536	0.595
Normal	56(93.3%)	38(95.0%)	18(90.0%)		
High	4(6.7%)	2(5.0%)	2(10.0%)		
Ki-67	53.58± 20.26	49.88± 21.14	61.00± 16.83	t=-2.049	0.055
EBER				c^2=1.579	0.544
Negative	3(5.0%)	3(7.5%)	0(0.0%)		
Positive	57(95.0%)	37(92.5%)	20(100.0%)		
PD-L1				c^2=0.000	1.000
<50%	24(40.0%)	16(40.0%)	8(40.0%)		
≥50%	36(60.0%)	24(60.0%)	12(60.0%)		
TNM stage				c^2=0.000	1.000
I-II	18(30.0%)	12(30.0%)	6(30.0%)		
III-IV	42(70.0%)	28(70.0%)	14(70.0%)		
SUVmax	11.13± 6.25	10.72± 6.36	11.96± 6.08	t=-0.718	0.476
MTV	24.91± 30.82	24.49± 34.58	25.73± 22.22	t=-0.146	0.885
TLG	120.69± 168.44	121.40± 192.47	119.27± 109.81	t=-0.46	0.964

Radiomics feature selection and predictive model construction

Through LASSO regression analysis (figure 3), three meaningful CT radiomic features and five PET radiomic features were taken out of the training cohort: CT _ Morphological _ Compactness 2, CT _ Morphological _ Centre Of Mass Shift, CT _ Intensity _ Histogram _ Maximum Histogram Gradient Grey Level, PET _ Morphological _ Compactness 2, PET _ Local _ Intensity _ Based _ Local Intensity Peak, PET _ Intensity-Histogram _ Intensity Histogram Skewness, PET _ Intensity _ Histogram _ Root Mean Square and PET _ GLCM _ Normalized Inverse Difference Moment (table 3).

Based on the screening results, CT and PET prediction models were constructed. In addition, the Rad score was calculated according to the Rad scoring formula (Radscore = $\sum^{8}_{i=1}(F_i \times \alpha_i)$, F: Radiomic features, α: Coefficient). Rad scores of high and low PD-L1 level groups within the training cohort respectively were 0.14±0.15 and -0.15±0.20. The distinction held statistical significance (t=-5.220, P=0.000; table 2). Therefore, we incorporated the SUVmax and Rad score to construct the combined predictive model with CT and PET radiomics.

Table 2. Univariate analysis of PD-L1 expression groupings in training cohort. (EBV, Epstein-Barr virus; EBER, EBV-associated RNA; PD-L1, programmed death ligand-1; SUVmax, maximum standardized uptake value; MTV, metabolic tumor volume; TLG, total lesion glycolysis; Rad).

Variables	PD-L1<50% (n=16)	PD-L1≥50% (n=24)	Statistics	P
Age(years)	50.63±9.92	52.83±12.93	t=-0.578	0.567
Sex			c^2=0.019	1.000
Male	11(68.8%)	16(66.7%)		
Female	5(31.3%)	8(33.3%)		
Smoking history			c^2=1.039	0.407
Smoker	12(75.0%)	21(87.5%)		
Never	4(25.0%)	3(12.5%)		
EBV-DNA			c^2=1.404	0.508
Normal	16(100.0%)	22(91.7%)		
High	0(0.0%)	2(8.3%)		
Ki-67	40.63±18.06	56.04±21.11	t=-2.39	0.022
EBER			c^2=0.961	0.553
Negative	2(12.5%)	1(4.2%)		
Positive	14(87.5%)	23(95.8%)		
TNM stage			c^2=8.750	0.005
I-II	9(56.3%)	3(12.5%)		
III-IV	7(43.8%)	21(87.5%)		
SUVmax	7.06±4.58	13.17±6.27	t=-3.342	0.002
MTV	10.67±10.84	33.71±41.58	t=-2.585	0.015
TLG	43.77±59.62	173.15±231.32	t=-2.613	0.014
Rad	-0.15±0.20	0.14±0.15	t=-5.220	0.000

Table 3. Coefficients of radiological characteristics identified through LASSO (least absolute shrinkage and selection operator) regression. (CT, computed tomography; PET, positron emission tomography; GLCM, gray-level co-occurrence matrixgray).

Number	Radiomic Features (F)	Coefficient(α)
1	CT_Morphological_Compactness2	0.048008
2	CT_Morphological_CentreOfMassShift	0.089310
3	CT_Intensity - Histogram _ Maximum HistogramGradientGreyLevel	-0.048243
4	PET_Morphological_Compactness2	-0.018537
5	PET_Local_Intensity_Based_LocalIntensityPeak	0.030335
6	PET_Intensity-Histogram _IntensityHistogramSkewness	0.014700
7	PET_Intensity-Histogram_RootMeanSquare	-0.040576
8	PET_GLCM_NormalisedInverseDifferenceMoment	0.069403

Evaluation and validation of the PD-L1 expression prediction models

As figure 4, the CT, PET, and combined models'

[Downloaded from ijrr.com on 2026-10-30]

[DOI: 10.61186/ijrr.23.2.26]

ROC curves employed to forecast PD-L1 presence level were mapped out. Within the training group, the CT, PET, and combined models' AUCs respectively were 0.837 (95% CI: 0.711-0.963), 0.852 (0.718-0.985), and 0.948 (0.887-1.000); the optimal thresholds were 0.64, 0.66, and 0.75, separately; the sensitivity and specificity at the optimal threshold were 75.0% and 81.3%, 83.3% and 81.3%, and 75.0% and 100%, separately. Within the validation group, the above three predictive models' AUCs respectively were 0.781 (95% CI: 0.576-0.987), 0.583 (0.317-0.850), and 0.802 (0.601-1.000); the optimal thresholds were 0.64, 0.62 and 0.66, separately; the sensitivity and specificity at the optimal threshold for each model separately were 58.3% and 100.0%, 66.7% and 62.5%, and 87.5% and 75.0%. The findings showed that the three predictive models performed well in terms of diagnosis, particularly the combined model, which had better predictive ability (AUCs of 0.948 and 0.802, respectively) within the training and validation sets; moreover, the sensitivity and specificity were also comparable.

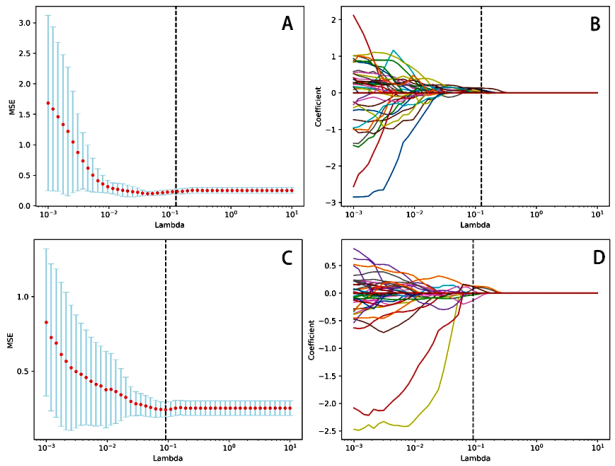


Figure 3. LASSO (least absolute shrinkage and selection operator) regression process. LASSO regression was used for radiomics feature selection, and the best lambda (λ) value was selected by tenfold cross-validation. In the figure, the ordinate "MSE" represents the mean square error, the ordinate "coefficient" refers to the radiomics feature coefficient, and the error bars is the standard deviation. **(A)** and **(B)** represent PET radiomics feature screening, and the best λ value is 0.125893, which is indicated by a dashed line. Similarly, **(C)** and **(D)** indicate CT radiomics feature extraction, and the best λ value is 0.091030.

Hosmer–Lemeshow tests were performed on the above three predictive models, and the calibration demonstrated acceptable performance (P>0.05; table 4). Furthermore, the Delong test was conducted, and as indicated in Table 4, there was no noteworthy difference among the three models' AUCs within the training cohort (P>0.05); however, the AUCs of the PET and combined models differed significantly within the validation cohort (Z=-2.587, P=0.010).

Figure 5 reveals the DCA results for models across the two cohorts. In the training cohort, the CT, PET, and combined models' probability thresholds were >34%, >12%, and >5%, respectively; the optimal threshold probabilities respectively were 0.64, 0.66, and 0.75; the NB values separately were 0.317, 0.354, and 0.450. In the validation cohort, the above three predictive models' probability thresholds separately were >38%, >48%, and >39%; the optimal threshold probabilities were 0.64, 0.62, and 0.66, separately; the NB values were 0.250, 0.155, and 0.256, separately. The DCA indicated that, for the majority of the appropriate threshold probability ranges, the combined model outperformed the two individual models. For every 100 patients, 13.3 more PD-L1 high-expression nasopharyngeal carcinoma patients were correctly detected using the combined model than via the CT model ((0.450-0.317)×100%=13.3), and 9.6 more than via the PET model ((0.450-0.354) ×100%=9.6).

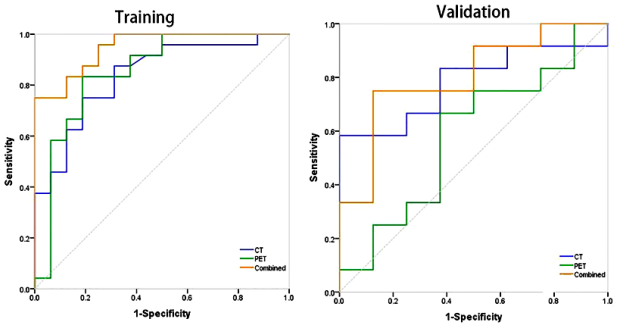


Figure 4. ROC (receiver operator characteristic) curves of the three models in the training and validation cohorts. In the figure, the abscissa "1-Specificity" also means false positive rate, the ordinate "Sensitivity" means true positive rate, the blue line represents the CT model, the green line represents the PET model, and the orange line represents the combined model.

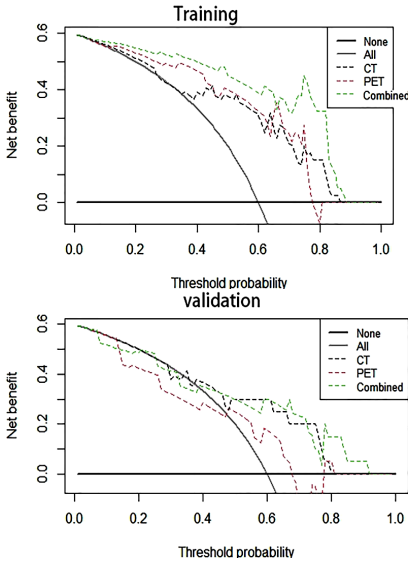


Figure 5. DCA (decision curve analysis) curves of the three models in the training and validation cohorts. In the figure, the black dotted line represents the CT model, the red dotted line represents the PET model, the green dotted line represents the combined model, and the two solid lines are special reference lines.

[Downloaded from ijrr.com on 2026-10-30]

[DOI: 10.61186/ijrr.23.2.26]

Table 4. Results of the Hosmer-Lemeshow and DeLong tests for the three models. (CT modle, the model based on CT radiomics features; PET modle, the model based on PET radiomics features; Combined modle, the model based on CT and PET radiomics features and SUVmax).

Modles	Training		Validation	
	Statistics	P	Statistics	P
Hosmer-Lemeshow test				
CT	c^2=5.491	0.704	c^2=3.903	0.866
PET	c^2=5.136	0.743	c^2=8.153	0.419
Combined	c^2=6.090	0.637	c^2=10.134	0.256
DeLong test				
CT and PET	Z=-0.166	0.8684	Z=1.175	0.240
CT and Combined	Z=-1.750	0.080	Z=-0.143	0.887
PET and Combined	Z=-1.741	0.081	Z=-2.587	0.010

DISCUSSION

Accurately predicting the PD-L1 status is crucial for developing effective clinical treatment strategies in NPC primary tumor. This approach is especially important for individuals with advanced nasopharyngeal cancer, as precise forecasting of PD-L1 high level can guide the use of combined immune blockade therapy for improved treatment efficacy and improved prognosis. Radiomics can provide more detailed information on tumor biology and the microenvironment complementing visual features through comprehensive quantification of tumor phenotypes and provides an emerging and noninvasive research method for current research. However, radiomic-related predictive models for PD-L1 expression status in NPC were not developed prior to our study, which may be related to significant geographical differences in the disease. Several studies, such as the research conducted by Zheng *et al*., have investigated PD-L1's expression level before surgery for neck and head squamous cell tumors, but the research did not include nasopharyngeal carcinoma patients. Additionally, the focus of the study was on traditional contrast-enhanced CT imaging omics, which does not involve relevant functional metabolic information [35, 36].

In our study, advanced imaging with ^{18}F-FDG PET/CT further reflected intratumor heterogeneity at the functional metabolic level [37]. Univariate analysis and multivariate logistic analysis ultimately revealed the SUVmax was a separate forecaster of the PD-L1 expression state, which was incorporated into the combined model. Previous research have found the positive relationship between FDG uptake and PD-L1 presence level in nasopharyngeal tumor cells [38, 39]. Increased FDG uptake is generally linked to the production of glucose transporter type 1 (GLUT1), Hypoxia-Inducible Factor-1α (HIF-1α), and phosphorylated Signal Transducer and Activator of Transcription 3 (pSTAT3) [38], while Latent Membrane Protein 1 (LMP1) of EBV can increase PD-L1 expression in tumor cells while increasing pSTAT3; conversely, blocking pSTAT3 can reduce LMP1-induced PD-L1 expression [39].

In this research, according to the radiomic characteristics of PET/CT before surgery in NPC patients and the above independent predictor SUVmax, we developed CT, PET and combined models of prediction for expression of PD-L1. The combined model had stable and good diagnostic performance and good clinical benefit. The CT model in the validation group was less sensitive, and the PET model's overall performance in the validation group was not as good as that in the training cohort, which might be mainly related to the insufficient robustness of the model because of the study's small sample size. In other studies of neck and head squamous cell tumors, Zheng's team constructed PD-L1 expression radiomics prediction models based on enhanced CT with large sample sizes; in the cohorts of training and validation, the model's AUCs in identifying PD-L1 positivity and negativity respectively were 0.802 and 0.852, additionally the AUCs for the model, distinguishing PD-L1 height and low, were 0.889 and 0.834, respectively [35, 36]. We hypothesize that endovascular contrast media improve the difference in density between diseased and normal tissue and provide blood supply to the lesion, which may help enhance the diagnostic performance and sensitivity of the model. In our future research, we may consider combining angiography with PET/CT imaging along with expanding the size of the sample.

In addition, studies predicting PD-L1 expression in other malignancies via ^{18}F-FDG PET/CT radiomics have focused mainly on NSCLC. In an initial PET/CT imaging study of 334 NSCLC patients, Zhao *et al.* reported that clinical stage was an important indicator of various PD-L1 expression, and their combined radiomics model's AUCs respectively were 0.769 and 0.718 within the groups of training and validation [22]. In another PET/CT radiomics study of 255 NSCLC patients, Li *et al.* constructed CT, PET, and combined models that predicted PD-L1 high and low status among their validation set, reaching respective AUCs of 0.661, 0.745, and 0.762, and the combined model outperformed the separate CT and PET models [40]. Compared to these studies, which included different tumor types, we constructed radiomic prediction models that included different features, but the prediction models integrating PET/CT radiomics characteristics and other risk factors had better diagnostic efficacy in predicting tumors PD-L1 level.

Within our study, the combined model based on PET/CT scans was the first non-invasive prediction model for PD-L1 expression in NPC; this model has good diagnostic performance and clinical application value. The finding preliminarily showed the PET/CT radiomic study's potential value for effectively estimating PD-L1 level in NPC, as in other malignancies [22, 23, 25]. Nonetheless, our study

[Downloaded from ijrr.com on 2026-10-30]

[DOI: 10.61186/ijrr.23.2.26]

encounters certain constraints, attributable to its retrospective design and limited sample size, and it is necessary to expand sample and carry out prospective multicenter research and validation in the future.

CONCLUSION

In this study, a combined model based on the independent predictor SUVmax and the radiomic characteristics of PET/CT was constructed to evaluate PD-L1 status in NPC and was found to be superior to CT or PET alone. This finding reveals that this combined model may be effective at predicting individuals with elevated PD-L1 expression, giving medical professionals a new strategy for screening patients who might benefit from immunotherapy.

ACKNOWLEDGEMENT

None.

***Ethical consideration*:** Ethical approval was waived by the local ethics committee in view of the retrospective nature of the study.

***Conflicts of Interest*:** The authors have disclosed that they have no affiliation with any businesses whose goods or services could be associated with the topic of this work.

***Funding*:** No specific grant was obtained for this work.

***Authors' contribution*:** All authors were involved similarly in research and preparation of the manuscript. All authors approved final manuscript for publication.

REFERENCES

1. Chen YP, Chan ATC, Le QT, *et al*. (2019) Nasopharyngeal carcinoma. *Lancet, **394**(10192): 64-80.*
2. Sung H, Ferlay J, Siegel RL, *et al*. (2021) Global Cancer Statistics 2020: GLOBOCAN estimates of incidence and mortality worldwide for 36 cancers in 185 countries. *CA Cancer J Clin, **71**(3): 209-249.*
3. Cao W, Chen HD, Yu YW, *et al*. (2021) Changing profiles of cancer burden worldwide and in China: a secondary analysis of the global cancer statistics 2020. *Chin Med J (Engl), **134**(7): 783-791.*
4. Xu M, Yao Y, Chen H, *et al*. (2019) Genome sequencing analysis identifies Epstein-Barr virus subtypes associated with high risk of nasopharyngeal carcinoma. *Nat Genet, **51**(7): 1131-1136*.
5. Lee AW, Ma BB, Ng WT, *et al.* (2015) Management of nasopharyngeal carcinoma: current practice and future perspective. *J Clin Oncol, **33**(29): 3356-3364.*
6. Colevas AD, Yom SS, Pfister DG, *et al.* (2018) NCCN Guidelines Insights: Head and Neck Cancers, Version 1.2018. *J Natl Compr Canc Netw, **16**(5): 479-490.*
7. Perri F, Bosso D, Buonerba C, *et al.* (2011) Locally advanced nasopharyngeal carcinoma: Current and emerging treatment strategies. *World J Clin Oncol, **2**(12): 377-383*.
8. Perri F, Della Vittoria Scarpati G, Caponigro F, *et al*. (2019) Management of recurrent nasopharyngeal carcinoma: current perspectives. *Onco Targets Ther, **12**: 1583-1591*.
9. Jung HA, Park KU, Cho S, *et al.* (2022) A phase II study of nivolumab plus gemcitabine in patients with recurrent or metastatic nasopharyngeal carcinoma (KCSG HN17-11). *Clin Cancer Res, **28**(19): 4240-4247.*
10. Hsu C, Lee SH, Ejadi S, *et al*. (2017) Safety and antitumor activity of pembrolizumab in patients with programmed death-ligand 1-positive nasopharyngeal carcinoma: Results of the KEYNOTE-028 study. *J Clin Oncol, **35**(36): 4050-4056*.
11. Ma BBY, Lim WT, Goh BC, *et al*. (2018) Antitumor activity of nivolumab in recurrent and metastatic nasopharyngeal carcinoma: an international, multicenter study of the mayo clinic phase 2 consortium (NCI-9742). *J Clin Oncol, **36**(14): 1412-1418*.
12. Fang W, Yang Y, Ma Y, *et al*. (2018) Camrelizumab (SHR-1210) alone or in combination with gemcitabine plus cisplatin for nasopharyngeal carcinoma: results from two single-arm, phase 1 trials. *Lancet Oncol, **19**(10): 1338-1350*.
13. Yang Y, Qu S, Li J, *et al*. (2021) Camrelizumab versus placebo in combination with gemcitabine and cisplatin as first-line treatment for recurrent or metastatic nasopharyngeal carcinoma (CAPTAIN-1st): a multicenter, randomised, double-blind, phase 3 trial. *Lancet Oncol, **22**(8): 1162-1174.*
14. Adkins DR and Haddad RI. (2022) Clinical trial data of Anti-PD-1/PD-L1 therapy for recurrent or metastatic nasopharyngeal Carcinoma: A review. *Cancer Treat Rev, **109**: 102428*.
15. Makowska A, Lelabi N, Nothbaum C, *et al*. (2021) Radiotherapy combined with PD-1 inhibition increases NK cell cytotoxicity towards nasopharyngeal carcinoma cells. *Cells, **10**(9): 2458.*
16. Tang LL, Chen YP, Chen CB, *et al.* (2021) The Chinese Society of Clinical Oncology (CSCO) clinical guidelines for the diagnosis and treatment of nasopharyngeal carcinoma. *Cancer Commun (Lond), **41**(11): 1195-1227*.
17. Ettinger DS, Wood DE, Aisner DL, *et al.* (2022) Non-small cell lung cancer, version 3.2022, NCCN clinical practice guidelines in oncology. *J Natl Compr Canc Netw, **20**(5): 497-530*.
18. Chiu HY, Chao HS, Chen YM. (2022) Application of artificial intelligence in lung cancer. *Cancers (Basel), **14**(6): 1370.*
19. Yin X, Liao H, Yun H, *et al*. (2022) Artificial intelligence-based prediction of clinical outcome in immunotherapy and targeted therapy of lung cancer. *Semin Cancer Biol, **86**(Pt 2): 146-159.*
20. Sun R, Limkin EJ, Vakalopoulou M, *et al.* (2018) A radiomics approach to assess tumor-infiltrating CD8 cells and response to anti-PD-1 or anti-PD-L1 immunotherapy: an imaging biomarker, retrospective multicohort study. *Lancet Oncol, **19**(9): 1180-1191.*
21. Zheng X, Yao Z, Huang Y, *et al*. (2020) Deep learning radiomics can predict axillary lymph node status in early-stage breast cancer. *Nat Commun, **11**(1): 1236.*
22. Zhao X, Zhao Y, Zhang J, *et al. (*2023) Predicting PD-L1 expression status in patients with non-small cell lung cancer using [18F]FDG PET/CT radiomics. *EJNMMI Res, **13**(1): 4.*
23. Lim CH, Koh YW, Hyun SH, *et al.* (2022) A Machine Learning Approach Using PET/CT-based radiomics for prediction of PD-L1 expression in non-small cell lung cancer. *Anticancer Res, **42**(12): 5875-5884.*
24. Shao J, Ma J, Zhang S, *et al*. (2022) Radiogenomic system for non-invasive identification of multiple actionable mutations and PD-L1 expression in non-small cell lung cancer based on CT images. *Cancers (Basel), **14**(19): 4823.*
25. Monaco L, De Bernardi E, Bono F, *et al.* (2022) The "digital biopsy" in non-small cell lung cancer (NSCLC): a pilot study to predict the PD-L1 status from radiomics features of [18F]FDG PET/CT. *Eur J Nucl Med Mol Imaging, **49**(10): 3401-3411.*
26. Wang C, Ma J, Shao J, *et al.* (2022) Non-invasive measurement using deep learning algorithm based on multi-source features fusion to predict PD-L1 expression and survival in NSCLC. *Front Immunol, **13**: 828560.*
27. Wang C, Ma J, Shao J, *et al.* (2022) Predicting EGFR and PD-L1 status in NSCLC Patients using multitask AI system based on CT images. *Front Immunol, **13**: 813072*.
28. Lo Gullo R, Wen H, Reiner JS, *et al*. (2021) Assessing PD-L1 expression status using radiomic features from contrast-enhanced breast MRI in breast cancer patients: Initial results. *Cancers (Basel), **13** (24): 6273.*
29. Shi W, Yang Z, Zhu M, *et al.* (2022) Correlation between PD-L1 expression and radiomic features in early-stage lung adenocarcinomas manifesting as ground-glass nodules. *Front Oncol, **12**: 986579.*
30. Tian Y, Komolafe TE, Zheng J, *et al.* (2021) Assessing PD-L1 Expression Level via Preoperative MRI in HCC based on integrating deep learning and radiomics features. *Diagnostics (Basel), **11**(10): 1875.*
31. Gu X, Yu X, Shi G, *et al.* (2023) Can PD-L1 expression be predicted by contrast-enhanced CT in patients with gastric adenocarcinoma? A preliminary retrospective study. *Abdom Radiol (NY), **48**(1): 220-228.*
32. Xie W, Jiang Z, Zhou X, *et al.* (2023) Quantitative radiological features and deep learning for the non-invasive evaluation of pro-

[Downloaded from ijrr.com on 2026-10-30]

[DOI: 10.61186/ijrr.23.2.26]

grammed death ligand 1 expression levels in gastric cancer patients: A digital biopsy study. *Acad Radiol, **30**(7): 1317-1328.*
33. Varghese B, Cen S, Zahoor H, *et al.* (2022) Feasibility of using CT radiomic signatures for predicting CD8-T cell infiltration and PD-L1 expression in renal cell carcinoma. *Eur J Radiol Open, **9**: 100440.*
34. Nioche C, Orlhac F, Boughdad S, *et al.* (2018) LIFEx: A freeware for radiomic feature calculation in multimodality imaging to accelerate advances in the characterization of tumor heterogeneity. *Cancer Res, **78**(16): 4786-4789*. (https:// doi.org/10.1158/0008-5472.CAN-18-0125)
35. Zheng YM, Yuan MG, Zhou RQ, *et al.* (2022) A computed tomography-based radiomics signature for predicting expression of programmed death ligand 1 in head and neck squamous cell carcinoma. *Eur Radiol, **32**(8): 5362-5370*.
36. Zheng YM, Zhan JF, Yuan MG, *et al.* (2022) A CT-based radiomics signature for preoperative discrimination between high and low expression of programmed death ligand 1 in head and neck squamous cell carcinoma. *Eur J Radiol, **146**: 110093.*
37. Aerts HJ, Velazquez ER, Leijenaar RT, *et al.* (2014) Decoding tumor phenotype by noninvasive imaging using a quantitative radiomics approach. *Nat Commun, **5**: 4006*.
38. Mano Y, Aishima S, Kubo Y, *et al.* (2014) Correlation between biological marker expression and fluorine-18 fluorodeoxyglucose uptake in hepatocellular carcinoma. *Am J Clin Pathol, **142**(3): 391-397*.
39. Fang W, Zhang J, Hong S, *et al*. (2014) EBV-driven LMP1 and IFN-γ up-regulate PD-L1 in nasopharyngeal carcinoma: Implications for oncotargeted therapy. *Oncotarget, **5**(23): 12189-12202.*
40. Li J, Ge S, Sang S, *et al.* (2021) Evaluation of PD-L1 expression level in patients with non-small cell lung cancer by 18F-FDG PET/CT radiomics and clinicopathological characteristics. *Front Oncol, **11**: 789014.*

[Downloaded from ijrr.com on 2026-10-30]

[DOI: 10.61186/ijrr.23.2.26]